OPEN ACCESS

GAVIN PUBLISHERS

Advances in Biochemistry and Biotechnology

Research Article

El-Shorbagy HM, et al Adv Biochem Biotechnol 3: 162.
DOI: 10.29011/2574-7258.000062

Magnetite Nanoparticles Induced Fetal Skeletal Abnormalities, DNA Damage and Down regulation of Pax-1 and Tgfb2 Genes in White Albino Rats

Haidan M. El-Shorbagy[1*], Fatma A. Eid[2], Nehal A. Abu Al-Naga[2], Entsar R. Abd-Allah[2], Akmal A. El-Ghor[1]

[1]Department of Zoology, Faculty of Science, Cairo University, Giza, Egypt

[2]Department of Zoology, Faculty of Science, Al-Azhar University, Nasr City, Egypt

[*]**Corresponding author:** Haidan M. El-Shorbagy, Department of Zoology, Faculty of Science, Cairo University, Giza, 12613, Egypt. Email: haidan@sci.cu.edu.eg

Citation: El-Shorbagy HM, Eid FA, Al-Naga NAA, Abd-Allah ER, El-Ghor AA (2018) Magnetite Nanoparticles Induced Fetal Skeletal Abnormalities, DNA Damage and Down regulation of Pax-1 and Tgfb2 Genes in White Albino Rats. Adv Biochem Biotechnol 3: 162. DOI: 10.29011/2574-7258.000062

Received Date: 19 March, 2018; **Accepted Date:** 23 April, 2018; **Published Date:** 01 May, 2018

Abstract

Objective: Magnetite Nanoparticles (MNPs) have been widely used as contrast agents and have promising approaches in anemia treatment of pregnant women. The aim of the present study was to detect the teratological, genotoxic effects of MNPs in the maternal, embryos and fetal liver or brain tissues and to investigate their effects on the expression of Pax-1 & Tgfb2 genes associated with the skeletal development.

Methods: Pregnant albino rats were administered orally with low and high doses of MNPs. Teratogenic analysis was performed on 20 days old fetuses, while DNA damage was assessed in the maternal liver and brain tissues, whole 14 days old embryos and in the liver tissues of 20 days old fetuses. In addition, gene expression of Pax1 and Tgfb2 was evaluated in 14 days old embryos.

Results: MNPs administration resulted in mild and severe effects on the skeletal formation in the developing fetuses. Comet assay showed significant DNA damage in the maternal and fetal liver tissue and in the 14 days old embryos. The expression of Tgfb2 and Pax-1 genes was significantly down regulated in the skull and vertebral column tissues of 14 days old embryos after MNPs treatment.

Conclusions: High doses of MNPs revealed some teratogenic and genotoxic effects and, hence, they should be administered with more care for the anemic pregnancy cases. However, Future investigations regarding MNPs' effects on the other developmental genes before further medical administrations are warranted.

Keywords: Comet Assay; Gene Expression; Magnetite Nanoparticles (MNPs); Pax-1; Tgfb2; Rats; Teratogenicity

Introduction

Fe_3O_4 Magnetite Nanoparticles (MNPs) possess unique physiological properties, including super-para magnetism. They have a number of interesting applications, particularly in the field of biomedical science such as drug delivery [1-4], contrast agents [5-7] and magnetic hyperthermia [8-10]. The World Health Organization (WHO) assessed that 41.8% of pregnant women were anemic due to iron deficiency [11], so low dose of MNPs (10 mg/kg) may offer some benefits to anemic mothers and developing fetuses [12]. Nevertheless, despite the numerous MNPs purposes being explored, currently available information on their potential toxicity is still controversial.

A study on the potential genotoxic effects of MNPs and showed DNA-protein crosslinks and oxidative DNA damage (8-hydroxyl deoxyguanosine) in hepatic and renal tissues of Kunming mice treated daily for 1 week with MNPs [13]. Moreover, examination of the genotoxic effects of MNPs in mice intratracheally instilled,

obtained significant increase in DNA adduct levels, DNA breaks and oxidative stress in the treated animals [14]. Similar genotoxic effects were detected using comet assay after MNPs treatment in alveolar A549 and bronchial epithelial BEAS-2B cells [15], embryonic kidney HEK-293 cells, peripheral blood lymphocytes [16], skin epithelial A431 cells [17], primary human leukocytes and human lymphoblastoid TK6 cells treated with oleate-coated nanomagnetite [18]. On the other hand, no *in vitro* DNA damage could be detected in different cell types [18-21].

Although MNPs showed no effects on fertility or early embryonic development, mild maternal toxicity and major fetal skeletal malformations were described in rabbits and rats treated with ferumoxtran-10 [22]. Recently, several doses of positively charged nanoparticles given for many days caused a significantly increased fetal death and iron accumulation in the liver and placenta of fetuses [23]. The same author showed that a high dose of MNPs induced fetal losses and morphological alternations of the uteri and testes of surviving offspring.

In mice, Pax-1 is essential for the construction of specific skeletal structures and for normal vertebral column development along the whole axis. Vertebral bodies and intervertebral discs were missed in Pax-1-deficient mice; the rib homologues and the proximal part of the ribs were lost as well or harshly malformed [24]. Pax-1 plays a redundant synergistic function in the sclerotomal cells' modeling and differentiation, that lead to the formation of Intervertebral Discs (IVD and vertebral bodies of the axial skeleton [25].

Tgfb2 gene expression is seen at the level of embryogenesis in several tissues as well as in precartilaginous blastema and a later growth zone of long bone, which indicates the effect of Tgfb2 on the skeletal formations [26,27]. Reduced Tgfb2 gene expression leads to developmental disorders concerning mainly facial skeleton, organs of vision and hearing, vertebral column or cardiovascular system [28].

Nevertheless, investigations of acute toxicity, reproductive toxicity and genotoxicity in diverse animal models resulted in unclear indication of MNPs safety until now, and epidemiological reports are nearly inexistent. The aim of the present study was to detect the teratological, genotoxic effects of MNPs in the maternal, embryos and fetal liver or brain tissues and to investigate their effects on the expression of Pax-1 and Tgfb2 genes associated with the skeletal development.

Material and Methods

Chemicals

Nanopowder, black, solid. Fe_3O_4 MNPs (≤ 20 nm) was obtained from Nanotech Egypt company for Photo Electronics (Cairo, Egypt). All other chemicals were of analytical grade and were purchased from Sigma-Aldrich (St. Louis, MO, USA). Other molecular kits are listed elsewhere. Physico-chemical properties of magnetite nanoparticles were characterized using High-Resolution Transmission Electron Microscope (HR-TEM, FEL, Tecnia G20), X-ray Diffraction (XRD, PanAnalytical, X pert Pro) and vibrating Sample Mgnetometer (VSM, Lakeshore 7410).

Experimental Animals

The present experimental study was carried out on 30 female Albino rats (*Rattus norvegicus*). The protocol was approved by the Institutional Animal Care and Use Committee (IACUC), Faculty of Science, Cairo University, Egypt (CUIF 6817). Females of 11-13 weeks old were selected for the present study and vaginal smears were prepared every morning and examined under the light microscope according to the method of [29] for 5 days to select those in the proestrus. Two females with regular estrus cycle were selected and caged together with one male overnight under controlled environmental conditions of temperature, humidity and light. The first day of gestation was determined by the presence of sperms in the vaginal smear [30].

Experimental Design

100 or 150 mg/kg/b,w of MNPs were suspended in 1ml distilled water. The suspensions were ultrasonicated before they were used to treat animals to avoid aggregation and provide an optimum size distribution for dispersed particles. In all experimental groups, MNPs were orally administered from 8th to the 13th or 16th day of gestation as the organogenesis period starts from 6th and ends at 15th day of gestation [31]. The animals were categorized into two main groups (A and B) according to the period of treatment and each group was divided into three subgroups (5 rats/group) as follows:

Group $A_{14:}$ Pregnant rats were orally administered MNPs daily from the 8th to the 13thday of gestation. Then, rats were sacrificed on day 14 of gestation (24 hours after last treatment). This group includes three subgroups.

$A_{14}C$: Representing the control group where pregnant rats were orally administered distilled water.

$A_{14}T_1$ (low dose group): Pregnant rats were orally administered 100mg /kg bw of MNPs.

$A_{14}T_2$ (high dose group): Pregnant rats were orally administered 150mg /kg bw of MNPs.

Group B_{20}: Pregnant rats were administered MNPs daily from the 8th to the 16thday of gestation. Then, rats were sacrificed on day 20 of gestation. This group includes three subgroups:

$B_{20}C$: Representing the control group where the pregnant rats were orally administered distilled water.

$B_{20}T_1$ (low dose group): Pregnant rats were orally administered100mg /kg bw of MNPs.

$B_{20}T_2$ (high dose group): Pregnant rats were orally administered150mg /kg bw of MNPs.

Tissue Distribution of Iron Oxide Nanoparticles

Using specific iron Prussian blue method [32], the accumulation of iron oxide nanoparticles appeared as dark blue grains under the light microscope. The distribution of iron oxide nanoparticles was evaluated in maternal liver and brain and embryonic liver tissues. Maternal liver and brain tissues, embryonic and fetal liver tissues were fixed in 4% paraformaldehyde buffered solution for 8 h, then the organs were dehydrated through serials of ethanol dilutions (70%, 80%, 90% and 100%), clarified in xylene and finally embedded in paraplast. Serials sections were cut at 5µm thickness and stained with Prussian blue method.

Teratological Parameters

- Weights of 20 days fetuses and placenta.
- Length of 20-days fetuses.
- Placental coefficient (weight of placenta/weight of fetus), was recorded on day20 of gestation.
- Skeletal examination: 20 days old fetuses were preserved in 100% ethyl alcohol and were stained with double staining of fetal skeletons for cartilage (Alcian blue) and bone (Alizarine red) according to the method described by Whitaker and Dix (1979).

DNA Damage Analysis by Comet Assay

The Single Cell Gel Electrophoresis (SCGE)/ alkaline comet assay was performed according to the method described by [33]. It was carried out using brain and liver tissues of pregnant rats, whole body of 14 days old embryos and liver tissue of 20 days old fetuses from the control and all the treated groups.

The fluorescent microscope (Carl Zeiss Axioplan with epiflourescence using filter 15 BP546/12, FT580 and LP590 was used to examine the slides. The extent of DNA migration for each sample was determined by simultaneous image capture and scoring of 50 cells at magnification 400x using Comet 5 image analysis software developed by Kinetic Imaging, Ltd. (Liverpool, UK). The images of comets were captured using a Closed-Circuit Digital (CCD) camera.

Pax-1 and Tgfb2 Gene Expression Analysis

RNA Extraction and cDNA Synthesis

Total cellular RNA was extracted from each frozen tissue sample using Gene JETTM RNA extraction Kit (Thermo scientific, USA) following the manufacturer`s instructions and was stored at -80˚C. RNA sample quality was assessed prior to cDNA synthesis by separation through agarose gel electrophoresis and staining with ethidium bromide. Total RNA concentration were determined by measuring the absorbance at 260 nm using a UV spectrophotometer, and were used as templates for efficient synthesis of first strand cDNA by using RevertAid ™ first Strand cDNA Synthesis Kit (Thermo Scientific, USA). Oligo (d T)

Quantitative Real-Time Polymerase Chain Reaction (q RT-PCR)

Reverse transcribed cDNAs were quantified by real-time PCR. Amplification of Pax-1, Tgfb2 and Gapdh genes was performed using SYBR green- based real-time PCR and was detected with 7500 Fast system (Applied Biosystem 7500, Clinilab, Egypt). For each PCR reaction, a mixture of total volume 25 µl contained 12.5 µl 2x Quanti Tect SYBR Green PCR Master Mix (Qiagen Inc, Valencia, USA), 2.5µL newly synthesized cDNA, 1 µL primer mixer and 8 µl PCR grade water. The thermal cycling condition comprised an initial heat activation step at 95˚C for 15 min followed by 40 cycles of denaturation at 95˚C for 15 s, annealing and elongation at 60˚C for Pax-1 and Gapdh, 61˚C for Tgfb2 for 1 min. The primer sequences used were designed using NCBI primer blast and stated in table 1. Each sample was prepared as triplicate for each one of the three genes. All signals were normalized to mRNA levels of the house keeping gene Gapdh, and expressed as RQ=2-ΔΔCt. Results were reported as Mean Standard Error (SE) of relative change compared to the untreated control [34].

Gene	Sense 5` - 3`	Antisense 5` - 3`	Product size (bp)
Gapdh	CCGCATCTTC TTGTGCAGTG	GGTAACCAGG CGTCCGATAC	93
Pax-1	AGTCAGCAACA TTCTGGGCA	CCATTCACTG CTGACGAGGT	144
Tgfb2	CTTTGGATGCC GCCTATTGC	CCCCAGCACAG AAGTTAGCA	138

Table 1: Primer sequences for Gapdh, Pax1 and Tgfb2 rat embryos cDNAs.

Statistical Analysis

The present data were analyzed by the aid of statistical package for the social science software (SPSS) version 18.0. Student`s t- test was used to illustrate mean value of weight and length of fetuses, weight of placenta and placental coefficient. The results for Student`s T-test or Analysis of Variance (ANOVA) was used to illustrate gene expression results and different comet parameters among groups. The results for the mRNA expression were represented compared to the control group as mean±Standard Error (SE) for three replicates [35]. P-value ≤ 0.05 was considered as statistical significance.

Results

Characterization of the Magnetite Nanoparticles

The HR-TEM image of the magnetite nanoparticles showed that the particles have average size of 20±2.0 nm with spherical shape (Figure 1, A). XRD phase analysis confirmed the phase formation of MNPs (Figure 1, B). VSM generated a hysteresis loop from which the saturation magnetization (Ms) was calculated under magnetic field lower than 20,000 Oersted (Oe) (Figure 1, C). The saturation magnetization of the product is 4.6 emu/g. The small saturation magnetization in our case is most likely attributed to the much smaller size of MNPs.

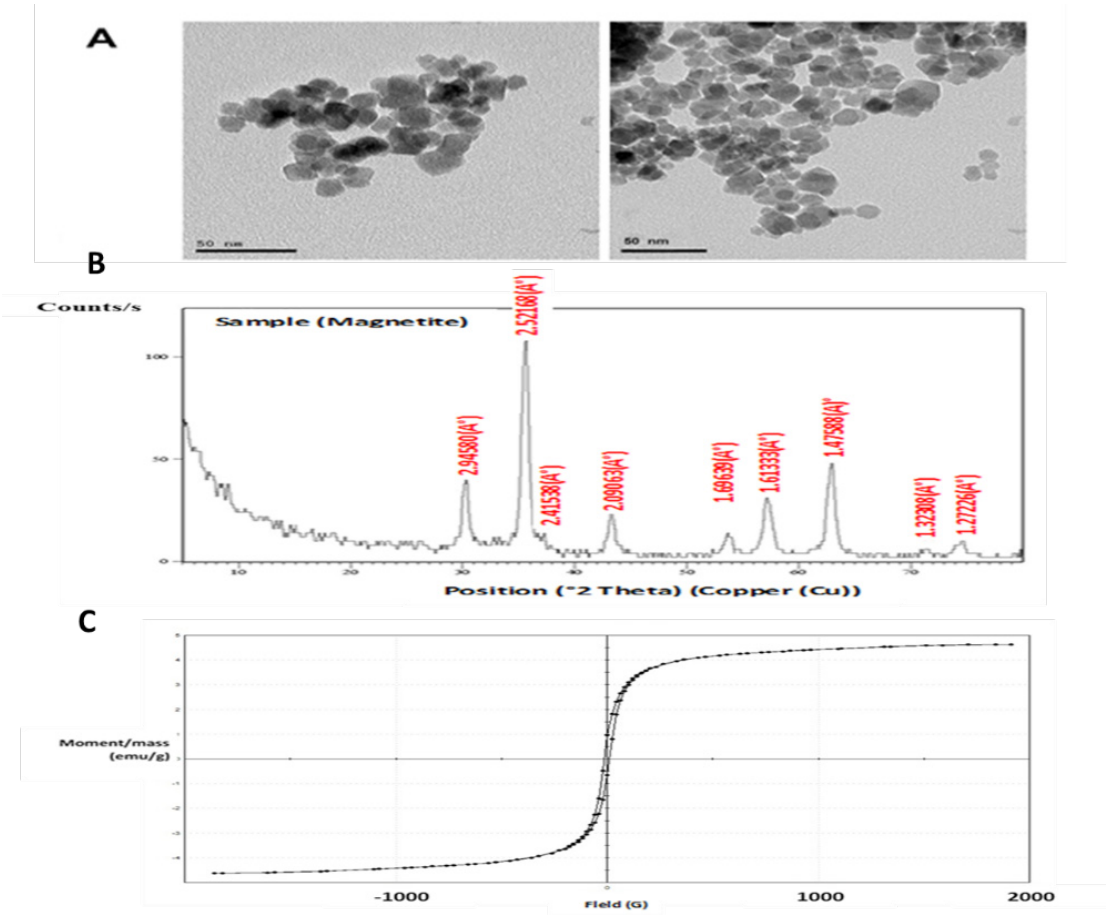

Figures 1(A-C): A. HR-TEM image of the prepared MNPs shows that MNPs have spherical shape with average size around 20nm. **B.** A graph represents the XRD pattern of synthesized MNPs shows the formation of Fe_3O_4 based on comparison with their XRD patterns and the standard pattern of Fe_3O_4 04- 013-9809. The diffraction peaks are identical to characteristic peaks of the Fe_3O_4 crystal as cubic spinal structure. **C.** Hysteresis loop obtained from VSM measurements of synthesized MNPs.

Tissue Distribution of MNPS in Maternal, Fetal and Embryonic Tissues

MNPs were detected in the maternal brain and liver tissues (Figure 2 (A&B)), liver tissues of 14 days old embryos and 20 days old fetuses (Figure 2 C) as dark blue grains.

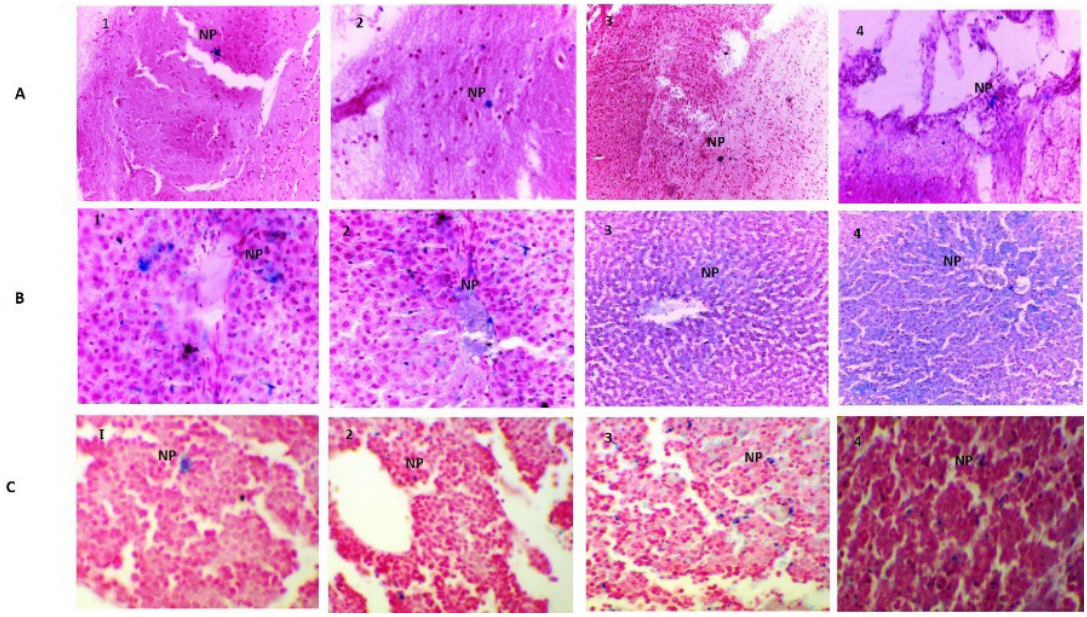

Figures 2(A-C): A. Photomicrographs of sections of maternal brain tissues stained with Prussian blue stain showing distribution of MNPs. A1: $A_{14}T_1$ group (x300), A2: $A_{14}T_2$ (x 300), A3: $B_{20}T_1$ (x 200) and A4: $B_{20}T_2$ group (x200). **B.** Photomicrographs of sections of maternal liver tissues stained with Prussian blue stain showing distribution of MNPs. B1 &B2: showing accumulation of MNPs in the blood vessels of the liver tissue of a pregnant rat of $A_{14}T_1$ & $A_{14}T_2$groups (x300) respectively. B3 and B4 showing accumulation of MNPs in the blood vessel, sinusoids and hepatocytes in the liver tissue of pregnant rats in ($B_{20}T_1$ (x200) & $B_{20}T_2$ (x200) respectively. **C.** Photomicrographs of sections of embryos and fetuses' liver tissues stained with Prussian blue stain. C1&C2: showing accumulation of MNPs in the sinusoids, hepatocytes and blood vessels in the liver tissues of embryos of $A_{14}T_1$ (x400) & $A_{14}T_2$ (x400) respectively. C3 &C4: showing numerous scattered MNPs in the hepatocytes, sinusoidal spaces and inside the central veins in the liver tissue of fetuses of $B_{20}T_1$ &$B_{20}T_2$ (x 400) respectively.

Teratological Parameters

Changes in weight gain of fetal body and placenta, fetal length

The results showed that there was no statistical significant difference (P≥0.05) in the mean value of fetuses' weight in $B_{20}T_1$ (42±1) and in $B_{20}T_2$ (29±1) groups when compared to the control group (54±1) (Table 2). In addition, there was a significant increase (P<0.01) in the mean value of placental weight and placental coefficient in the treated groups when compared with their corresponding values in the control group (Table 2).

Regarding fetal length**,** on day 20 of gestation, there was a statistical significant decrease in the mean value of fetal length in $B_{20}T_2$ group when compared to their corresponding values in the control group (Table 2).

Parameters	$B_{20}C$	$B_{20}T_1$ (100mg/kgbw)	$B_{20}T_2$ (100mg/kgbw)
Average number of living fetuses / per five mothers	8.60±0.89	5.8*0±2.28	5.4*0±1.60
Average number of dead fetuses/per five mothers	0.20±0.44	0.80±1.30	1.4*±1.34
Average number of placenta/per five mothers	8.80±0.83	6.6**0±1.14	6.8**0±3.03
Average weight of fetuses	2.50±0.35	2.38±0.52	2.18±0.08
% of change		-4.8	-12.8
Average weight of placenta	0.44±0.08	0.66**±0.11	0.72**±0.04
% of change		50	63.63

Placental coefficient	0.18±0.01	0.28**±0.01	0.33**±0.01
Average body length of fetuses	3.24±0.23	3.08±0.37	2.98*±0.17
% of change		-4.93	-8.02
Data are represented as mean±Standard Deviation (SD). The values are considered significant at *P ≤ 0.05 and **P≤ 0.01 compared to the control group			

Table 2: Effect of MNPs on the average number of living fetuses / per five mothers, weight gain of fetuses and placenta at the 20th day of gestation.

Skeletal Anomalies

- **$B_{20}C$ group:** The cleared chondrification and bone preparation of control rat fetuses indicated complete chondrification and ossification in all parts of the axial skeleton (skull, vertebrae and ribs), as well as appendicular skeleton (fore and hind limbs, pectoral and pelvic girdles). Cranium of control fetuses revealed well ossification (Figures 3, A1, and B1&C1). The sternum showed well ossified segments **(**Figure 4A1). The vertebral column was well ossified (Figure 4B1). Fore limb skeleton was well developed (Figure 4C1). Pelvic girdle and hind limbs were well ossified (Figures 5A1&B1).
- **$B_{20}T_1$ group**: Fetuses from pregnant rats of this group showed less ossification in the frontal, parietal and interparietal bones, supra occipital, ex occipital and occipital condyles bones (Figures 3, A2, B2 & C2). Some segments of the sternum remained cartilaginous (Figure4A2). No malformations could clearly have detected either in axial or in the appendicular skeleton.
- **$B_{20}T_2$ group:** Skeletal malformations were observed in 20 days old fetuses demonstrated by less ossification with high porosity in the frontal, parietal and interparietal bones. A large suture was detected between the two parietal bones, and a large portion of parietal and interparietal bones remained cartilaginous (Figure 3A3, 3B3). Absence of ossification center in the supra occipital and lack of ossification in the supra occipital, ex-occipital and occipital condyles bones were detected (Figure 3C3). A delay in the ossification of large portion of supra occipital bone was observed (Figures. 3B3, 3C3). Large number of sternal segments remained cartilaginous (Figure 4A3). Most neural arches and centers of vertebrae were less ossified with presence of wavy ribs (Figure 4B2). Incomplete ossification was demonstrated in the humerus, radius and ulna. Absence of the third metacarpal was also explored (Figure 4C2). Some portions of ileum, ischium and pubis remained cartilaginous. Only three sacral vertebrae were present, and all caudal vertebrae remained cartilaginous (Figure 5A3). Less ossification the femur, tibia and fibula were detected and the third metatarsal remained cartilaginous as well (Figure 5B2).

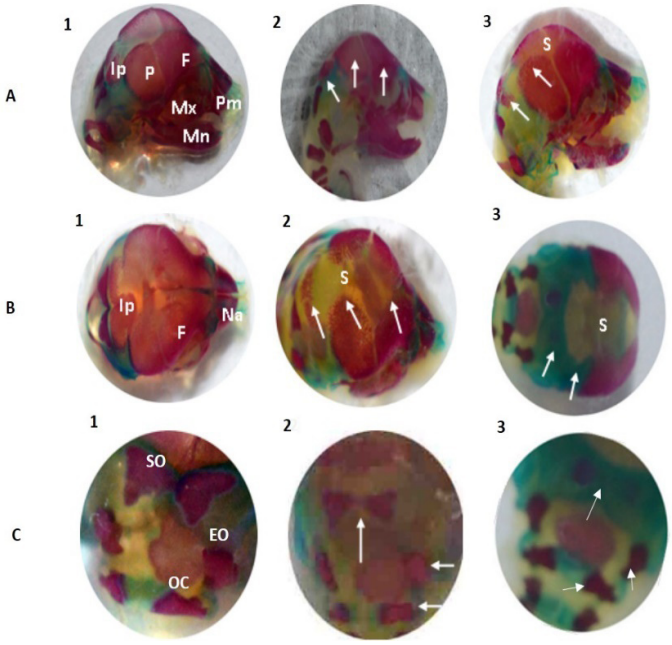

Figures 3(A-C): A. Photographs of the cranium of rat fetuses (Lateral view) at the 20th day of gestation stained with Alizarin red-S and Alcian blue. A1; control group showing well ossification of Frontal (F), Parietal (P), Interparietal (IP), Na =Nasal, Mx=Maxilla and Mn=Mandible (x3.2), A2 $B_{20}T_1$ group; showing less ossification of the frontal, parietal and interparietal bones (x3.3), A3; Showing abnormalities of $B_{20}T_2$ group including less ossification and porosity of parietal and interparietal bones with large Suture (S) between two parietal bones (x3.7). **B.** Photographs of the cranium of rat fetuses (dorsal view) at the 20th of gestation stained with Alizarin red-S and Alcian blue. B1; control group (x5.3), B2; $B_{20}T_1$ group showing less ossification and porosity of the frontal, parietal and interparietal bones with large Suture (S) between two parietal bones (x6.2), B3; A large portion of parietal, interparietal and supra occipital bones remain cartilaginous in $B_{20}T_2$ group (x5). **C.** Photographs of the occipital region of rat fetuses at the day 20th of gestation stained with Alizarin red-S and Alcian blue. C1: control group showing conspicuous ossification in the Supra Occipital (SO), Ex Occipital (EO) and Occipital Condyles (OC) (x10), C2; absence of ossification center in the supra occipital bones with lack of ossification in the ex-occipital and occipital condyles in $B_{20}T_2$ group (x 9), C3; a large portion of supra occipital bone, ex occipital and occipital condyles remain cartilaginous in $B_{20}T_2$ group (x8).

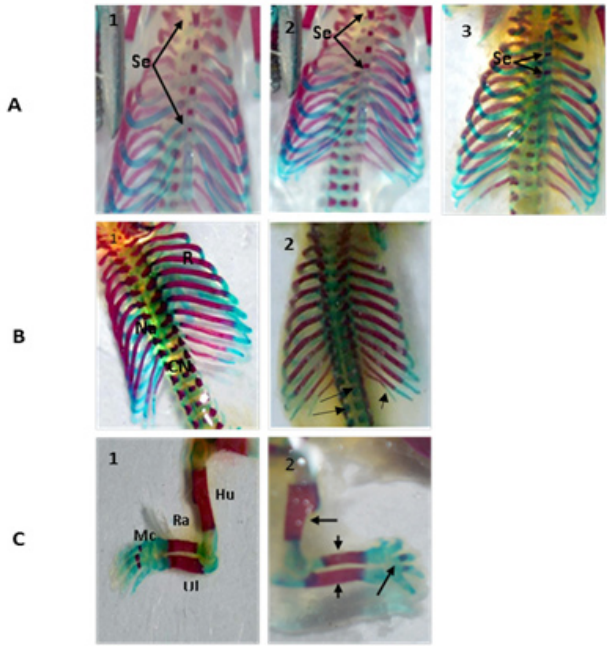

Figures 4 (A-C): A. Photographs of the sternum region of rat fetuses at day 20th day of gestation stained with Alizarine red S and Alcian blue (bones in red and cartilage in blue): A1; Control group showing the six-segmented sternum (Se) (x4), A2; $B_{20}T_1$ group showing the four-segmented sternum (x4), A3; $B_{20}T_2$ group showing segmented sternum (x3). **B.** Photographs of the ribs of rat fetuses at day 20th of gestation stained with Alizarine red S and Alcian blue. B1; control group showing conspicuous ossification in the Neural arches (Na) and Ribs (R) and Centrum of Vertebrae (CN) (x5), B2: neural arches and centers of vertebrae remain cartilage and presence of wavy ribs in $B_{20}T_2$ group (x3). **C.** Photographs of the forelimb (fore arm, wrist and hand) of rat fetuses at day 20th of gestation stained with Alizarine red S and Alcian blue. C1; control group showing conspicuous ossification in the Humerus (Hu), Radius (Ra) Ulna (Ul) and three Metacarpals (Mc) (x5.3), C2: less ossification in the humerus, radius and ulna and some metatarsals remain cartilage in $B_{20}T_2$ group (x5).

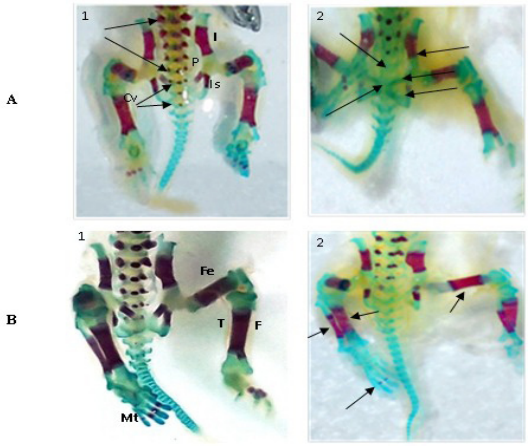

Figures 5(A-B): A. Photographs of the dorsal view of the pelvic girdle of rat fetuses at the 20th day of gestation stained with Alizarine red S and Alcian blue showing pelvic bones, sacral and caudal vertebrae. A1; control group showing good ossification of the pelvic bones (ileum, ischium and pubis), five Sacral Vertebrae (SV) and three Caudal Vertebrae (CV) (x4), A2: showing delay in ossification in ileum, pubis and ischium, some sacral vertebrae and all caudal vertebrae in $B_{20}T_2$ group (x5.8). **B.** Photographs of the ventral view of pelvic girdle of rat fetuses at the 20th day of gestation stained with Alizarine red S and Alcian blue showing pelvic bones and hind limb (femur, shank and foot). B1; control group showing good ossification in the pelvic bones and hind limb (Fibula (F), Tibia (T) and Metatarsus (Mt)) (x4), B2: less ossification of femur, tibia, fibula and pelvic girdle and some metatarsals remain cartilage in $B_{20}T_2$ group (x3.3).

Assessment of genotoxicity of MNPs by Comet Assay

With the exception of $A_{14}T_1$ group in maternal liver cells that showed no significant change in DNA% in tail or tail moment when referred to the control group, all other MNPs-treated groups showed significant increase ($P \leq 0.01$) of all DNA damage parameters (tail length, % DNA in tail and tail moment) in all treated groups ($A_{14}T_1$, $A_{14}T_2$, $B_{20}T_1$ and $B_{20}T_2$) in comparison with

the control group ($A_{14}C$ and $B_{20}C$) within maternal liver or brain cells, whole embryonic cells and fetal liver cells (Figure 6).

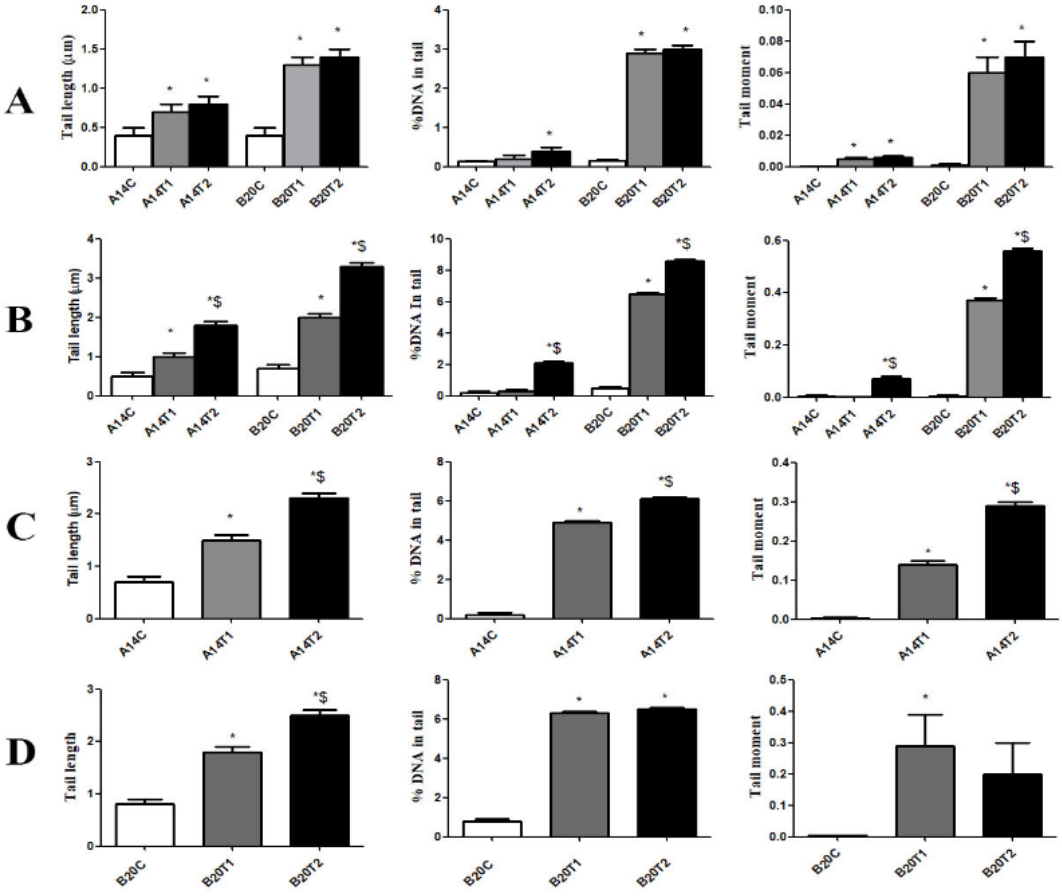

Figure 6: DNA damage measured as tail length, % DNA in tail and tail moment in different groups. Results are expressed as mean±SE, (*) significant difference compared to control at $P \leq 0.05$ using T- test. (A) DNA damage in maternal brain cells. (B): DNA damage in maternal liver cells. ($) statistically significant compared with $A_{14}T_1$ or $B_{20}T_1$ groups at $P \leq 0.05$ using T- test. (C): DNA damage in 14 days old embryos. ($) statistically compared with $A_{14}T_1$ group at $P \leq 0.05$ using T- test. (D): DNA damage in liver of 20 days old fetuses. ($) statistically compared with $B_{20}T_1$ group at $P \leq 0.05$ using T- test.

Levels of Pax-1 and Tgfb2 Genes Expression

Expression levels of Pax-1 and Tgfb2 genes were significantly **(**$P \leq 0.05$) decreased in the $A_{14}T_1$ and $A_{14}T_2$ groups when compared to the control group. Expression at $A_{14}T_2$ group showed significant decrease ($P \leq 0.05$) when compared to that at $A_{14}T_1$ group, indicating that high dose of iron oxide nanoparticles plays an important role in decreasing mRNA level of both Pax-1 and Tgfb2 genes (Figure 7)

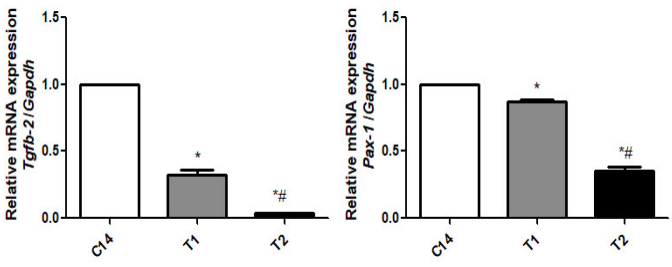

Figure 7: Quantitative real time PCR of Tgfb2 and Pax-1 genes after normalization to the Gapdh gene. The mRNA ratios of Tgfb2 and Pax-1 to Gapdh were calculated using the ΔΔCt method after normalization to Gapdh gene. Results are expressed as mean±SE, (*) significant difference with respect to the negative control at P≤0.05 using T-test and (#) statistically compared with $A_{14}T_1$ group.

Discussion

In the current study, MNPs appeared as dispersed blue granules in the maternal brain and liver tissues and liver tissues of embryos and fetuses. These results indicated that MNPs can penetrate through the membrane of different cells and even brain barrier and blood placenta barrier and pass to the liver of embryos and fetuses. These findings are in agreement with those of [36] who worked on mice and proved that Fe_3O_4 coated with Dimercaptosuccinic Acid (DMSA) was passed through the cell membrane and blood-placental barriers and entered the liver of the developing fetus**.** In addition, [37] found that the major iron accumulation was detected in the liver (93%) and only a small fraction was found in the lungs (5%) and in the spleen (2%).

Results of the present study revealed that there was no statistical significant difference (P≥0.05) in the mean value of fetal weight in gestation day 20 in $B_{20}T_1$ or $B_{20}T_2$ groups when compared with the control group. This is in accordance with [36] who observed that MNPs coated with Dimercaptosuccinic Acid (DMSA) intraperitoneally injected to pregnant mice had apparently no effect on the weight of the fetuses. This finding disagrees with the results of Khodarahmi who observed a significant decrease in the weight of 16-day mice fetuses after intraperitoneal maternal injection with Nano iron oxide (20nm in diameter) on day 9 of pregnancy. This may be contributed to the type of the coated material and/or the difference of animal species [38].

The significant decrease in the mean value of fetal length at the 20th day of gestation within $B_{20}T_2$ group that has been proven in this study, which agree with that of Khodarahmi who observed a significant decrease in the length of 16 days old mice fetuses after maternal treatment with intraperitoneal injection with nano iron oxide (20nm in diameter) on day 9 of pregnancy [38]. Taken together, MNPs-treatment induced changes in the growth of the placenta, exposes embryos and/or fetuses to altered levels of nutrients, and this may be partially responsible for the decreased fetal length observed on GD 20.

In the current study, there was a statistical significant decrease in the mean number of living fetuses in both $B_{20}T_1$ and $B_{20}T_2$ groups when compared to the control group. These results disagree with those of Noori who found that iron oxide nanoparticles injection had apparently no effect on the number of the living fetuses [36].

Oral injection of MNPs caused some mild and severe defects in the skeletal formation in the developing fetuses. This is in agreement with Bourrinet who mentioned that ferumoxtran-10 had major fetal skeletal malformations in both rabbits and rats [22]. Tsay stated that bone loss has been detected after increased iron ions concentration in mice. Their results revealed dose-dependent elevation of iron content in tissue with bone composition alteration and thinning of trabecular and cortical bone accompanied by high bone resorption; this may be contributed to the increased Reactive Oxygen Species (ROS) production [39].

Furthermore, Comet assay demonstrated that MNPs induced marked DNA damage in maternal and fetal liver tissues, whole 14-day embryos and 20 days old fetuses. This was in accordance with Al Faraj who performed a longitudinal study on Balb/c mice intrapulmonary administered iron oxide nanoparticles (PEG-coated magnetite modified with negative (carboxyl) or positive (amine) terminal), and detected a significant elevation in lipid peroxidation and DNA damage of lung in both acute and sub-acute sets [40].Often, genotoxicity of MNPs was attributed to the oxidation of Fe^{2+} into Fe^{3+} ions that induces DNA damage. Magnetite has been shown to cause high level of oxidative DNA lesions detected using comet assay in A549 human lung epithelial cell line [41]. Also, a concentration dependent DNA damage was detected in Super Para Iron Oxide Nanoparticles (SPION) treated L-929 fibroblasts cells [42].

Moreover, iron oxide nanoparticles could pass through the membrane of different cells and even blood-placental barrier, entered the 14- day embryos and fetus, and caused DNA damage. On the other hand, Piccinetti observed that silica-coated magnetite nanoparticles do not induce any toxicity in zebrafish larvae exposed through food for up to 15 days [43].

Transforming Growth Factor β (TGFβ) is known to play vital roles in multiple developmental processes. One of the main functions is its role in the skeletal development [44]. The expression of transforming growth factors beta 1, beta 2 and beta 3 genes during mouse embryogenesis from 9.5 to 16.5 days post coitus appear to be involved in chondroossification, and thus author in the present study have chosen to evaluate Tgfb2 expression on day 14 of gestation. Mice with a germline deletion of the Tgfβ2 ligand as well as TGFβ2/3 double knockout mice presented with defective frontal and parietal bone development, which is consistent with our results [45, 46]. In our study, there was significant decrease

(P≤0.05) in the mRNA level of Tgfb2 in the treated groups on day 14 of gestation when compared to the control group and the mRNA level was lower in the $A_{14}T_2$ group than in $A_{14}T_1$ group, that can be associated with the severe imperfections in 20-days old fetal skull especially in frontal, parietal, interparietal and occipital bones.

Similarly, Pax1 is essential for the formation of specific skeletal structures. After Pax1 expression from 9 to 12 days p.c, the perichordal tube displays a segmental plan of loosely and densely packed areas. As soon as the alternating pattern of intervertebral disk and vertebrae centrum is established, Pax1 transcript accumulation declines to diminished levels in 17 days p.c. embryos [47], and that's the reason for evaluating Pax-1 on day 14 of gestation. In humans, the Pax1 locus has been linked to otofaciocervical syndrome, idiopathic scoliosis, and to a higher susceptibility for androgenic alopecia [48]. Pax1 mutations were accomplished with severe malformation in tail and lumber region indicates that its actions may be strongest in these areas [49]. Indeed, mouse with mutant Pax1 exhibit highly malformed vertebral columns with missing (or split) vertebral bodies, absence of intervertebral disks, and lack or severely deformed proximal ribs [50]. Pax1 is involved in transducing proliferative signals from the notochord to sclerotome cells during skeleton formation. Thus, the lack of Pax 1 expression could be responsible for the reduced proliferation rate found in mutant chondrocytes [51]. In our study, MNPs down-regulated Pax-1 gene resulting in severe defects in 20-day fetal vertebral column such as the reduction of vertebral components, wavy ribs, presence of cartilaginous centers of vertebrae, absence of some sacral vertebrae, absence of caudal vertebrae and less ossifies ribs. Also, the results showed absence of some bony segments of the sternum. Up till now, there was no more recent data on the effects of MNPs on the Pax-1 and Tgfb2 genes *in vivo*.

Conclusion

The tested doses of MNPs could induce teratogenic, genotoxic and histological effects, as well as alteration of some developmental genes in pregnant rats and their embryos and fetuses, which needs much more investigations before applying MNPs in the biomedical applications for pregnant women.

References

1. Maver U, Bele M, Makovec D, Campeli S, Jamnik J, et al. (2009) Incorporation and release of drug into/from superparamagnetic iron oxide nanoparticles. J Magn Magn Mater 321: 3187-3192.
2. Hajba L, Guttman A (2016) The use of magnetic nanoparticles in cancer theranostics: Toward handheld diagnostic devices. Biotechnol Adv 34: 354-361.
3. Shevtsov MA, Multhoff G (2016) Recent developments of magnetic nanoparticles for theranostics of brain tumor. Curr Drug Metab 17: 737-744.
4. Stegar J, Ban I, Gradisnik L, Maver U (2017) Novel drug delivery system based on NiCu nanoparticles for targeting various cells. J. Sol-Gel Sci Techn.
5. Singh A, Sahoo SK (2014) Magnetic nanoparticles: a novel platform for cancer theranostics. Drug Discov Today 19: 474-481.
6. Orlando T, Mannucci S, Fantechi E, Conti G, Tambalo S, et al. (2016) Characterization of magnetic nanoparticles from *Magnetospirillum gryphiswal* dense as potential theranostics tools. Contrast media & molecular imaging 11: 139-145.
7. Wang S, Yang W, Du H, Guo F, Wang H, et al. (2016) Multifunctional reduction-responsive SPIO&DOX-loaded PEGylated polymeric lipid vesicles for magnetic resonance imaging-guided drug delivery. Nanotechnology 27: 165101.
8. Long NV, Yang Y, Teranishi T, Thi CM, Cao Y, et al. (2015) Biomedical Applications of Advanced Multifunctional Magnetic Nanoparticles. J Nanosci Nanotechnol 15: 10091-10107.
9. Munoz de Escalona M, Saez-Fernandez E, Prados JC, Melguizo C, et al. (2016) Magnetic solid lipid nanoparticles in hyperthermia against colon cancer. Int J Pharm 504: 11-19.
10. Suriyanto Ng, EY, Kumar SD (2017) Physical mechanism and modeling of heat generation and transfer in magnetic fluid hyperthermia through Neelian and Brownian relaxation: a review. Biomedical engineering online 16: 36.
11. World Health Organization WHO (2012) Guideline: Daily iron and folic acid supplementation in pregnant women; WHO Press: Geneva, Switzerland.
12. Di Bona KR, Xu Y, Gray M, Fair D, Hayles H, et al. (2015) Short-and long-term effects of prenatal exposure to iron oxide nanoparticles: influence of surface charge and dose on developmental and reproductive toxicity. Int J Mol Sci 16: 30251-30268.
13. Lu M, Cohen MH, Rieves D, Pazdur R (2010) FDA report: ferumoxytol for intravenous iron therapy in adult patients with chronic kidney disease. American journal of hematology 85: 315-319.
14. Totsuka Y, Ishino K, Kato T, Goto S, Tada Y, et al. (2014) Magnetite nanoparticles induce genotoxicity in the lungs of mice via inflammatory response. Nanomaterials 4: 175-188.
15. Kain J, Karlsson H, Möller L (2012) DNA damage induced by micro- and nanoparticles-interaction with FPG influences the detection of DNA oxidation in the comet assay. Mutagenesis 27: 491-500.
16. Gomaa IO, Kader MHA, Eldin TAS, Heikal OA (2013) Evaluation of *in vitro* mutagenicity and genotoxicity of magnetite nanoparticles. Drug Discov Ther 7: 116-123.
17. Ahamed M, Alhadlaq HA, Alam J, Khan MA, Ali D, et al. (2013) Iron oxide nanoparticle-induced oxidative stress and genotoxicity in human skin epithelial and lung epithelial cell lines. J Curr Pharm Des 19: 6681-6690.
18. Magdolenova Z, Drlickova M, Henjum K, Rundén-Pran E, Tulinska J, et al. (2015) Coating-dependent induction of cytotoxicity and genotoxicity of iron oxide nanoparticles. Nanotoxicology 9: 44-56.
19. Singh N, Jenkins GJ, Nelson BC, Marquis BJ, Maffeis TG, et al. (2012) The role of iron redox state in the genotoxicity of ultrafine superparamagnetic iron oxide nanoparticles. Biomaterials 33: 163-170.

20. Couto D, Sousa R, Andrade L, Leander M, Lopez-Quintela MA, et al. (2015) Polyacrylic acid coated and non-coated iron oxide nanoparticles are not genotoxic to human T lymphocytes. Toxicol lett 234: 67-73.

21. Paolini A, Guarch CP, Ramos López D, de Lapuente J, Lascialfari A, et al. (2016) Rhamnose-coated superparamagnetic iron oxide nanoparticles: an evaluation of their *in vitro* cytotoxicity, genotoxicity and carcinogenicity. J Appl Toxicol 36: 510-520.

22. Bourrinet P, Bengele HH, Bonnemain B, Dencausse A, Idee JM, et al. (2006) Preclinical safety and pharmacokinetic profile of ferumoxtran-10, an ultra-small superparamagnetic iron oxide magnetic resonance contrast agent. Invest Radiol 41: 313-324.

23. Di Bona KR, Xu Y, Ramirez PA, DeLaine J, Parker C, et al. (2014) Surface charge and dosage dependent potential developmental toxicity and bio distribution of iron oxide nanoparticles in pregnant CD-1 mice. Reproductive Toxicology 50: 36-42.

24. Wilm B, Dahl E, Peters H, Balling R, Imai K (1998) Targeted disruption of Pax1 defines its null phenotype and proves haploinsufficiency. Proc Nati Acad Sci U S A 95: 8692-8697.

25. Sivakamasundari V, Kraus P, Sun W, Hu X, Lim SL, et al. (2017) A developmental transcriptomic analysis of Pax1 and Pax9 in embryonic intervertebral disc development. Biol Open 6: 187-199.

26. Gatherer D, Ten Dijke P, Baird DT, Akhurst RJ (1990) Expression of TGF-beta isoforms during first trimester human embryogenesis. Development 110: 445-460.

27. Blobe GC, Schiemann WP, Lodish HF (2000) Role of transforming growth factor β in human disease. N Engl J Med 342: 1350-1358.

28. Heupel K, Sargsyan V, Plomp JJ, Rickmann M, Varoqueaux F, et al. (2008) Loss of transforming growth factor-beta 2 leads to impairment of central synapse function. Neural development 3: 25.

29. Cora MC, Kooistra L, Travlos G (2015) Vaginal cytology of the laboratory rat and mouse: review and criteria for the staging of the estrous cycle using stained vaginal smears. Toxicol pathol 43: 776-793.

30. Goldman JM, Murr AS, Cooper RL (2007) The rodent estrous cycle: characterization of vaginal cytology and its utility in toxicological studies. Birth Defects Research (Part B) 80: 84-97.

31. Khalaf AA, Morgan A, Mekawy M, Ali M (2007) Developmental toxicity evaluation of oral aluminum in rats. J Egypt Soc Tox 37: 11-26.

32. Garcia MP, Parca RM, Chaves SB, Silva LP, Santos AD, et al. (2005) Morphological analysis of mouse lungs after treatment with magnetite-based magnetic fluid stabilized with DMSA. Journal of magnetism and magnetic materials 293: 277-282.

33. Nandhakumar S, Parasuraman S, Shanmugam M, Rao KR, Chand P, et al. (2011) Evaluation of DNA damage using single-cell gel electrophoresis (Comet Assay) J Pharmacol Pharmacother 2: 107.

34. Yuan JS, Reed A, Chen F, Stewart CN (2006) Statistical analysis of real-time PCR data. BMC Bioinformatics 7: 85.

35. Ye W, Xu P, Jen R, Feng E, Zhong S, et al. (2011) Zeranol down-regulates P53 expression in primary cultured human breast cancer epithelial cells through epigenetic modification. Int J Mol Sci 12: 1519-1532.

36. Noori A, Parivar K, Modaresi M, Messripour M, Yousefi MH, et al. (2011) Effect of magnetic iron oxide nanoparticles on pregnancy and testicular development of mice. African Journal of Biotechnology 10: 1221-1227.

37. Ruiz A, Hernandez Y, Cabal C, Gonzalez E, Veintemillas-Verdaguer S, et al. (2013) Bio distribution and pharmacokinetics of uniform magnetite nanoparticles chemically modified with polyethylene glycol. Nanoscale 5: 11400-11408.

38. Khodarahmi P, Hayati Roodbari N, Parinar K, Sadeghian M (2016) Effect of Iron Oxide Nanoparticles on the Lung of NMRI Mouse Embryos *in vivo*. Zums J 24: 94-106.

39. Tsay J, Yang Z, Ross FP, Cunningham-Rundles S, Lin H, et al. (2010) Bone loss caused by iron overload in a murine model: importance of oxidative stress. Blood 116: 2582-2589.

40. Al Faraj A, Shaik AP, Shaik AS (2015) Effect of surface coating on the biocompatibility and *in vivo* MRI detection of iron oxide nanoparticles after intrapulmonary administration. J Nanotoxicology 9: 825-834.

41. Singh N, Jenkins GJ, Asadi R, Doak SH (2010) Potential toxicity of superparamagnetic iron oxide nanoparticles (SPION) Nano Rev 1: 5358.

42. Hong SC, Lee JH, Lee J, Kim HY, Park JY, et al. (2011) Subtle cytotoxicity and genotoxicity differences in superparamagnetic iron oxide nanoparticles coated with various functional groups. Int J Nanomedicine 6: 3219-3231.

43. Piccinetti CC, Montis C, Bonini M, Laura R, Guerrera MC, et al. (2014) Transfer of silica-coated magnetic (Fe_3O_4) nanoparticles through food: a molecular and morphological study in zebrafish. Zebrafish 11: 567-579.

44. Seo HS, Serra R (2009) Tgfbr2 is required for development of the skull vault. Developmental biology 334: 481-490.

45. Dunker N, Krieglstein K (2000) Targeted mutations of transforming growth factor-beta genes reveal important roles in mouse development and adult homeostasis. Eur J Biochem 267: 6982–6988.

46. Sanford LP, Ormsby I, Gittenberger-de Groot AC, Sariola H, Friedman R, et al. (1997) TGFbeta2 knockout mice have multiple developmental defects that are non-overlapping with other TGFbeta knockout phenotypes. Development 124: 2659-2670.

47. Verbout AJ (1985) The development of the vertebral column. Adv Anat Embryol Cell Biol 90: 1-122.

48. Feederle R, Gerber JK, Middleton A, Northrup E, Kist R, et al. (2016) Generation of Pax1/PAX1-Specific Monoclonal Antibodies. Monoclonal antibodies in immune diagnosis and immunotherapy 35: 259-262.

49. Koseki H, Wallin J, Wilting J, Mizutani Y, Kispert A, et al. (1993) A role for Pax-1 as a mediator of notochordal signals during the dorsoventral specification of vertebrae. Development 119: 649-660.

50. Wallin J, Wilting J, Koseki H, Fritsch R, Christ B, et al. (1994) The role of Pax-1 in axial skeleton development. Development 120: 1109-1121.

51. Furumoto TA, Miura N, Akasaka T, Mizutani-Koseki Y, Sudo H, et al. (1999) Notochord-dependent expression of MFH1 and PAX1 cooperates to maintain the proliferation of sclerotome cells during the vertebral column development. J Dev Biol 210: 15-29.